Electronic and magnetic properties of two-dimensional of FeX (X = S, Se, Te) monolayers crystallize in the orthorhombic structures

Electronic and magnetic properties of two-dimensional of FeX (X=S, Se, Te) monolayers crystallize in the orthorhombic structures

A. Bafekry,[1,2,*] I. Abdolhosseini Sarsari,[3] M. Faraji,[4] M. M. Fadlallah,[5] H. R. Jappor,[6] S. Karbasizadeh,[3] Chuong V. Nguyen,[7] and M. Ghergherehchi[8]

[1]*Department of Radiation Application, Shahid Beheshti University, Tehran 1983969411, Iran*
[2]*Department of Physics, University of Antwerp, Groenenborgerlaan 171, B-2020 Antwerp, Belgium*
[3]*Department of Physics, Isfahan University of Technology, Isfahan, 84156-83111, Iran*
[4]*Micro and Nanotechnology Graduate Program, TOBB University of Economics and Technology, Sogutozu Caddesi No 43 Sogutozu, 06560, Ankara, Turkey*
[5]*Department of Physics, Faculty of Science, Benha University, 13518 Benha, Egypt*
[6]*Department of Physics, College of Education for Pure Sciences, University of Babylon, Hilla 51002, Iraq*
[7]*Department of Materials Science and Engineering, Le Quy Don Technical University, Hanoi 100000, Vietnam*
[8]*College of Electronic and Electrical Engineering, Sungkyunkwan University, Suwon 16419, Korea*

In this letter, we explore the lattice, dynamical stability, electronic and magnetic properties of FeTe bulk and FeX (X=S, Se, Te) monolayers using the density functional calculations. Phonon dispersion relation, elastic stability criteria, and cohesive energy results show the stability of studied FeX monolayers. The mechanical properties reveal that all FeX monolayers have brittle nature. Furthermore, these structures are stable and as we move down the 6A group in the periodic table, i.e., from S, Se and Te. The stability and work function decrease as the electronegativity decreases. The spin-polarized electronic structures demonstrate that the FeTe monolayer has a total magnetization of 3.8 μ_B, which is smaller than the magnetization of FeTe bulk (4.7 μ_B). However the FeSe and FeS are nonmagnetic monolayers. The FeTe monolayer can be a good candidate material for spin filter applications due to its electronic and magnetic properties. This study highlights the bright prospect for the application of FeX monolayers in electronic structures.

I. INTRODUCTION

Graphene discovery has prompted immense scientific and theoretical attempts in two-dimensional (2D) van der Waals (vdW) materials, which offer perfect platforms for the study of previously unavailable properties and the creation of multifunctional instruments. This discovery, in conjunction with the family of transition metal chalcogenides (TMDs), opened the portal to layered two-dimensional materials and significant success was achieved on two-dimensional materials.[1] The long-range magnetic order can be found in bulk materials but not in 2D materials.[3] However, the magnetic vdW materials have a magnetic ground state even in the monolayer structures due to the magnetic anisotropies.[4] Needless to say, manifold 2D materials have been developed with different properties such as topological, superconducting, magnetic, metallic, and semiconducting.[5–8] For the dramatically spreading 2D vdW family, good steps have been made in the newly identified 2D vdW ferromagnetic structures. Lately, 2D magnetic material has attracted a lot of attention as it provides a perfect stage for discovering magnetism down to the thickness of the atomic layer.[9] The exploration of 2D magnetic materials is essential to understand spin actions within 2D restrictions and hence can allow comprehensive spintronic applications resulting in high storage devices to nanoscale quantum devices.[10,11] Unlike traditional magnetic bulk materials and their thin film counterparts, these 2D magnetic materials have very unusual properties and also create various physical effects.[12] For example, ferromagnetic orders with Curie temperature larger than 300 K was generated accidentally by Fe_3GeTe_2 using the ionic gating method.[13] Besides, in $Cr_2Ge_2Te_6$ and CrI_3 nanostructures, ferromagnetism depended on the layer with off-plane anisotropy was obtained at low temperatures.[11,14]

Minor changes in the concentration structural iron-based materials can have a significant impact on their magnetic and electronic characteristics. In a related, the iron-chalcogenide crystals are a category of magnetic materials including FeS, FeSe, and FeTe. A variety of magnetic phenomena including antiferromagnetism, ferrimagnetism, and ferromagnetism can be approved by manipulating the chalcogen elements (Se, S, and Te).[15–18] Furthermore, iron-chalcogenides often demonstrate several structural phases with different characteristics.[19,20]

The iron dichalcogenides FeX (X = S, Se, Te) are characteristically crystallized either in a tetragonal or hexagonal crystal structure with space groups P4/nmm and P63/mmc, respectively.[9,21] The hexagonal structures of FeSe and FeS exhibit strong magnetism, and the tetragonal structure show merely rudimentary antiferromagnetism and experimental results demonstrate its superconductivity whenever doped. But, the hexagonal FeTe is far less magnetic than the hexagonal FeSe and FeS.[21,22] Due to their fascinating magnetic properties, iron chalcogenides are a promising candidate for lithium-ion battery,[23,24] energy storage and conversion,[25,26] the spintronic and magnetic semiconductor.[27,28]

For low dimensional structures, thin film and monolayer, FeS and FeSe were familiar as superconductors.[29–32] On the other hand, FeTe is

non-superconductive at ambient pressure with an antiferromagnetic at ground-state[33,34] although the FeTe thin films are superconducting at 13 K under tensile stress.[35] Hence, the examination of low-dimensional materials with such a specific crystalline structure and a greater anisotropy helps to explain the magnetic and superconductivity of these materials. One of the most significant aspects of Fe-chalcogenides is their phase tunability which mostly comes directly from the inequality in the formation energy between the tetragonal and hexagonal phases of these materials.[36,37] The extensive tunability of these structures through various phases makes these monolayers desirable to exploring not only the applications of superconductivity but also to study quantum effects in general. Even though the hexagonal form is much simpler to fabricate than the tetragonal form, the recent experimental reports prospered in manufacturing a high-quality monolayer film of tetragonal FeS by the combined method of molecular-beam epitaxy with topotactic reaction.[38] Notably, the study demonstrated the resemblances in the electronic structure of FeS and FeSe monolayer, with the absence of high-temperature superconductivity monolayer FeS. Besides, FeSe monolayer films were prepared by the extensive annealing procedure, and they showed strong hints of superconductivity at transition temperatures greater than 65 K.[39] Overall, the strong of superconductivity depends on the conditions of preparation.[40,41]

Despite these findings, the structural, electronic and magnetic properties of FeX (X=S, Se, Te) monolayers have not yet fully understood. Therefore, we shed light on this issue throughout this work using first principle calculations. We examined the stability, structural, mechanical, and electronic of FeX (X=S, Se, Te) monolayers. This study may open a way of constructing high speed and nanoelectronics devices. Besides, the newly identified properties are predicted to be capable of unveiling characteristics and applications of the highest importance.

II. METHOD

The density-functional theory (DFT) calculations in this work are performed using the plane-wave basis projector augmented wave (PAW) method along with generalized gradient approximation (GGA) with Perdew-Burke-Ernzerhof(PBE)[42,43] functional as implemented in the Vienna *ab-initio* Simulation Package (VASP).[44,45] The kinetic energy cut-off of 500 eV was set for plane-wave expansion and the optimized structures are obtained until the variation in the energies falls below 10^{-8} eV. To get optimized structures, the total Hellmann-Feynman forces were reduced to 10^{-7} eV/Å. A 21×21×1 Γ centered k-point sampling was used for the primitive unit cells by using Monkhorst-Pack.[46] Charge transfers analysis is accomplished using the Bader technique.[47] A $\sim$ 20 Å vacuum space along the z-direction was used to avoid any fictitious interactions in monolayers. Van der Waals (vdW) correction proposed by Grimme (DFT-D2) to describe the long-range vdW interactions.[48] The phonon spectra were obtained from the displacement method as implemented in the PHONOPY code.[49]

III. FeTe BULK PROPERTIES

The geometrical atomic structure of FeTe bulk in the different views is shown in Fig. 1(a). The calculated lattice constant of FeTe bulk is 3.86 Å, while the Fe-Te bond length is 2.66 Å. The lattice constant and bond length values are in good agreement with the previous experimental and theoretical results.[50,51] Notice that the two angles of Te-Fe-Te are 86°, resulting in a high anisotropic lattice. From the theoretically predicted STM images, it is easy to recognize and correlate them with the corresponding atomistic structure (see Fig. 1(b)). One can see that the Te atoms are brighter than the Fe ones. In order to explain the origin of the electronic states, spin-polarized band structure, the corresponding density of states (DOS) and projected DOS (PDOS) are shown in Fig. 1(c). We find the total magnetization of the unit cell for FeTe tetragonal bulk state 4.67 μ_B which meets the Stoner criterion and agrees well with the previous calculations.[51] According to the Hund rule, the coupling

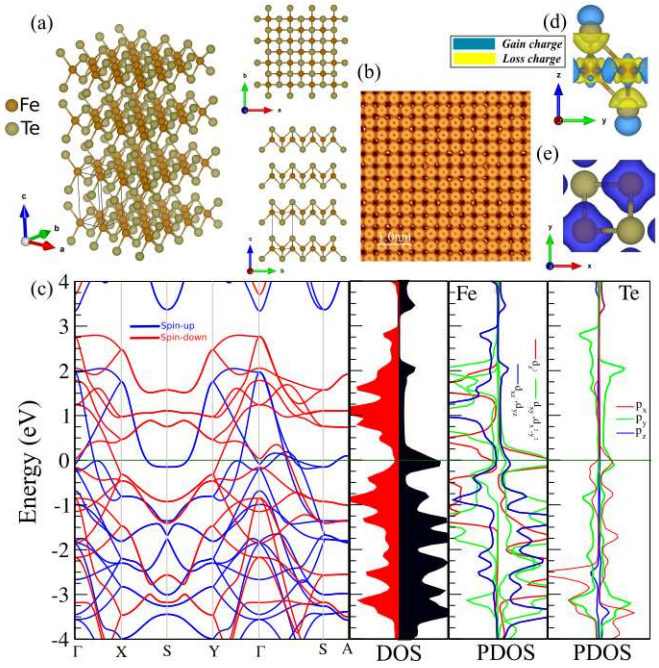

Figure 1. (a) Different views of atomic structure, (b) simulated STM images, (c) electronic band structure, density of states (DOS) and projected DOS (PDOS), (d) difference charge density and (e) difference spin density of FeTe bulk. The blue and yellow regions represent the ↑ and ↓ spin states, respectively. The zero of energy is set to Fermi-level.

is strong which leads to a large magnetic moment formed around each Fe atom. The crystal field splitting imposed by Te (p) orbital is weak, and the Fe ($3d$) orbitals hybridize strongly with each other. The hybridization between spin-up states of Te ($5p_x$, $5p_y$) and Fe ($3d_{z^2}$) around the Fermi energy involves mediating the exchange interactions in the FeTe tetragonal bulk. The difference charge density of FeTe bulk are shown in Figs. 1(d). From Figs. 1(d), we can see that Te atoms are negatively charged and surrounded by Fe positively charged atoms. The difference spin density of FeTe bulk is shown in Fig. 1(e), which the blue and yellow regions represent the ↑ and ↓ spin states, respectively. It is clear that the magnetism is originated from Fe atoms and large magnetic moment formed around each Fe atom.

IV. FeX MONOLAYER

The top and side views of atomic structures of FeX (X=S, Se, Te) monolayers are shown in Figs. 2(a-c). Notice that, the orthogonal primitive unit cell indicated by a black line is formed by four atoms and the vectors $\vec{\mathbf{a}} \neq \vec{\mathbf{b}}$ are the translational unit cell vectors. The calculated lattice parameters for the FeS, FeSe, and FeTe monolayers are 3.56 Å, 3.62 Å, and 3.58 Å, respectively, which are smaller than the corresponding lattice parameters of bulk

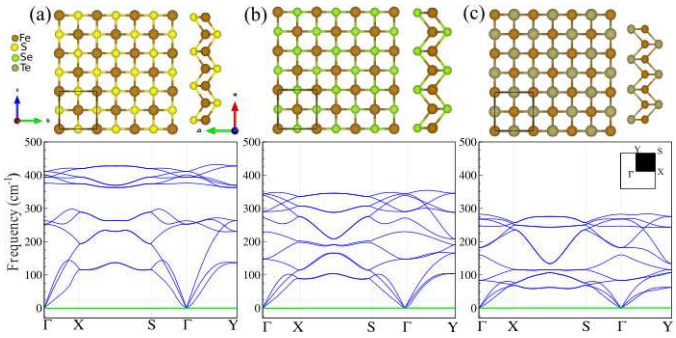

Figure 2. Top and side wies of atomic structures of (a) FeS, (b) FeSe and (c) FeTe monolayers. Phonon band dispersion with corresponding structure is shown in the bottom panel. The primitive unit cell indicated by a black rectangular.

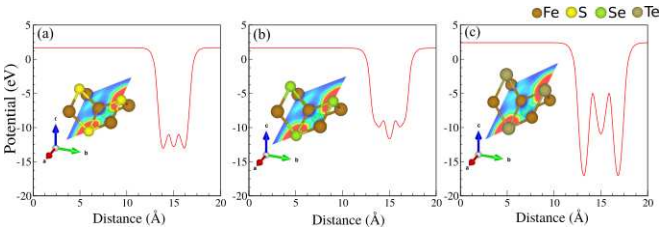

Figure 3. Planar average potential of (a) FeS, (b) FeSe and (c) FeTe monolayers. Contour plot of the electron localization function (ELF) indicated as insests. Red (blue) color indicate high (low) electron density.

structures.[50,51] Our results show that the bond lengths of Fe-X atoms in the studied monolayers are determined to be, 2.16 Å, 2.96 Å, and 2.56 Å for X=S, Se, and Te, respectively. While the bond angles of Fe-X-Fe are calculated to be 110.76°, 104°, and 88.74° for X=S, Se, and Te, respectively. The thickness of FeS, FeSe, and FeTe monolayers are 2.45 Å, 2.82 Å, and 3.66 Å, respectively. The structural parameters including bond length, bond angle, and thickness are listed in table I. The cohesive energy per atom was calculated as follows:

$$E_{coh} = \frac{E_{tot} - 2E_X - 2E_{Fe}}{4}, \tag{1}$$

where E_{tot}, E_X, and E_{Fe} represent the total energy, energies of isolated X (S, Se, and Te), and Fe atoms, respectively, and 4 is the total number of atoms in the unit cell. The cohesive energies of FeS, FeSe, and FeTe monolayers are found to be -11.57 eV/atom, -10.60 eV/atom, and -9.97 eV/atom, respectively. This finding indicates that the formation of FeS monolayer is more favorable than other monolayers due to the higher electronegativity of S (2.58) as compared to the electronegativity of Se (2.55) and Te (2.10).

The dynamical stabilities of FeX monolayers are verified by calculating their phonon band dispersions through the whole BZ which are presented as the bottom panel in Figs. 2(a-c). Apparently, phonon branches are free from any imaginary frequencies indicating the dynamical stability of the structures. For FeS dispersion curves, the bottom Fig. 2(a), the full line indicates the frequencies as a function in wave vectors for a given direction, for example, ΓX for the left part. The degenerate modes at Γ point, split into three branches in the directions ΓX and ΓS and two branches in the direction ΓY. One transverse branch is related to atomic modulations which is parallel to the wave vector for the two other branches. The 3N-3 optical modes which are related to the out of phase atomic movements are found at the higher energy. The gap is found in the phonon dispersions for FeS. Regarding FeSe and FeTe, the phonon dispersions do not have a gap and the displacement (movement) of atoms occurs in a small range of frequencies as compared to FeS can be attributed to the large atomic mass of Se and Te as compared to S atom.

The dynamical stabilities of FeX monolayers are verified by calculating their phonon band dispersions through the whole BZ which are presented as the bottom panel in Figs. 2(a-c). Apparently, phonon branches are free from any imaginary frequencies indicating the dynamical stability of the structures. For FeS dispersion curves, the bottom Fig. 2(a), the full line indicates the frequencies as a function in wave vectors for a given direction, for example, ΓX for the left part. At the Γ point of the Brillouin Zone, in the 4-atom primitive cell of FeX structures, there are totally 12 phonon branches 9 of which are optical. Three of the optical phonons are non-degenerate ZO modes while the remaining 6 are degenerate in-plane phonon modes. The degenerate modes at Γ point, split

Table I. Structural and electronic parameters of FeX (X=S, Se, Te) monolayers including lattice constants a; bond length between Fe-X atoms d; thickness defined by the difference between the largest and smallest z coordinates of X atoms (t); bond angles between Fe-X-Fe atoms θ; cohesive energy per atom, (E_{coh}); charge transfer (ΔQ) from X atom to Fe atom; work function (Φ) magnetic moment M_{tot}; bulk modulus (B); shear modulus (S); Young's modulus (Y); Poisson's ratio (ν)); and bulk/shear ratio (BS), respectively.

	a (Å)	d (Å)	t (Å)	θ (°)	E_{coh} (eV/atom)	ΔQ (e)	Φ (eV)	M_{tot} (μ_B)	B (GPa)	S (GPa)	Y (GPa)	ν	BS
FeS	3.56	2.16	2.45	110.76	-11.57	0.55	4.82	0.0	7.54	4.73	11.74	0.24	1.59
FeSe	3.62	2.96	2.82	104.10	-10.60	0.36	4.35	0.0	6.38	3.96	9.84	0.24	1.61
FeTe	3.58	2.56	3.66	88.74	-9.97	0.15	4.18	3.8	6.30	3.87	9.63	0.25	1.62

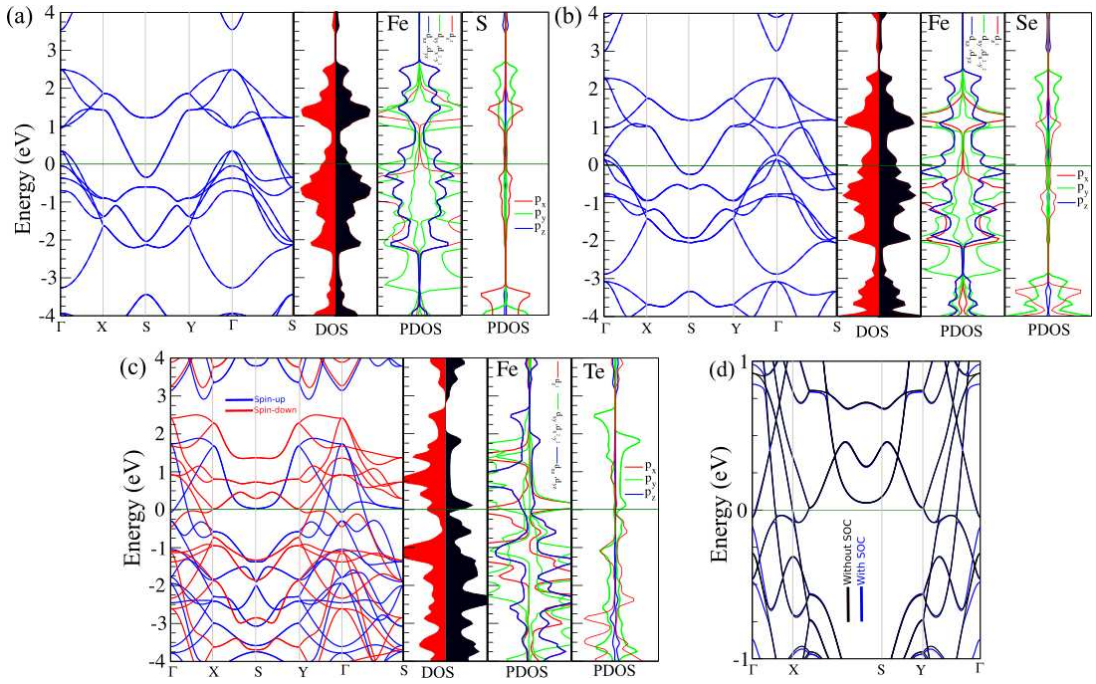

Figure 4. Electronic band structure with corresponding DOS and PDOS of (a) FeS, (b) FeSe and (c) FeTe monolayers. (d) Electronic band structure of FeTe monolayer without/with spin-orbit coupling. The zero of energy is set to Fermi-level.

into three branches in the directions ΓX and ΓS and two branches in the direction ΓY. One transverse branch is related to atomic modulations which is parallel to the wave vector for the two other branches. The 3N-3 optical modes which are related to the out of phase atomic movements are found at the higher energy. The gap is found in the phonon dispersions for FeS. Regarding FeSe and FeTe, the phonon dispersions do not have a gap and the displacement (movement) of atoms occurs in a small range of frequencies as compared to FeS can be attributed to the large atomic mass of Se and Te as compared to S atom. As we analyze the Raman active phonon modes in all three structures, in each monolayer it is found that 6 of the optical branches are Raman active. These modes are named as (from the group symmetry), E_g^1 and E_g^2 which are in-plane doubly-degenerate phonon modes and the A_1g and B_1g stand for the out-of-plane non-degenerate optical phonon branches. The frequencies of the Raman active phonon modes are given in the table below;

Turning to the last method to study the stability of FeX is mechanical stability. In the harmonic approximation framework, we find FeX structure has six independent elastic constants. The FeX structures verify the conditions of the elastic stability criteria[52] which means the FeX structures have mechanical stability. The mechanical parameters: bulk modulus (B), shear modulus (S), Young's modulus (Y), Poisson's ratio (ν), and bulk/shear ratio (BS) using Voigt Reuss-Hill approximation[53] (see table I) are calculated by using the elastic constants. The bulk modulus (B) refers to the ability of FeX structure to resist the compression under the applied external force. We find B equals 7.54 GPa, 6.38 GPa, and 6.30 GPa for X=S, Se, and Te restrictively. Therefore the FeS monolayer is the best one that can resist the compression as compared to the other monolayers. This result is confirmed by calculating Young's modulus values which are

Table II. The calculated phonon frequencies of the Raman active phonon modes at the *Gamma* point of the BZ.

	Structure	E_g^1 (cm^{-1})	E_g^2 (cm^{-1})	A_1g (cm^{-1})	B_1g (cm^{-1})
FeS	255	406	371	257	
FeSe	146	335	219	265	
FeTe	90	285	168	267	

11.74 GPa, 9.84 GPa, and 9.63 GPa for X=S, Se, and Te, respectively.

The Shear modulus (S) represents the immovability of the shape change, as the S increases the rigidity of FeX increases. The calculated values of S are 4.73 GPa, 3.96 GPa, 3.87 GPa for X=S, Se, and Te, respectively, which indicate that FeS has more immovable as compared to FeS and FeTe monolayer. The B/S ratio describes the ductile or brittle nature of the FeX structure. The B/S ratio is 1.59, 1.61, 1.62 for X=S, Se, and Te respectively. Therefore all FeX monolayers have brittle nature because B/S values are less than 1.75.[54] The calculated Poissons's ratio is confirmed the brittle behavior of FeX monolayers. We find ν values of FeX are less than 0.33.[55]

The planar average potential of FeS, FeSe, and FeTe monolayers are shown Figs. 3(a-c). The contour plot of the electron localization function (ELF) are shown as insests. The red and blue colors indicate high and low electron density, respectively. We found that the electrostatic potentials of studied monolayers are flat in the vacuum region. The work function was calculated using $\Phi = E_{vacuum} - E_F$. The calculated work functions for the FeS, FeSe, and FeTe monolayers are 4.82, 4.35, and 4.18 eV, respectively, which decrease as the electronegativity of X atom decreases. The difference charge density ($\Delta\rho$) is defined as: $\Delta\rho = \rho_{tot} - \rho_{Fe} - \rho_X$ where ρ_{tot}, ρ_{Fe} and ρ_X are the charge densities of the FeX, Fe and isolated X atoms, respectively. Notice that each S, Se, and Te atoms labeled, gains about $0.55e$, $0.36e$ and $0.15e$ from the adjacent Fe atoms in FeS, FeSe, and FeTe monolayers, respectively. It is clear that S, Se, and Te atoms are negatively charged and surrounded by Fe positively charged atoms. As the electronegativity of X atom decreases the charge transfer decreases.

V. ELECTRONIC AND MAGNETIC PROPERTIES

The spin-polarized electronic band structure of FeTe, FeSe and FeS monolayer structure is shown in Fig. 4, respectively. We find the total magnetization of FeTe tetragonal monolayer is 3.80 μ_B which is smaller than the corresponding value of its bulk structure. The FeS monolayer and bulk are nonmagnetic structures. For FeSe, the monolayer is nonmagnetic while the FeSe bulk has a 2.6 μ_B magnetic moment.[51] Projecting the density of states onto the five $3d$ orbitals of Fe and three $5p$ orbitals of

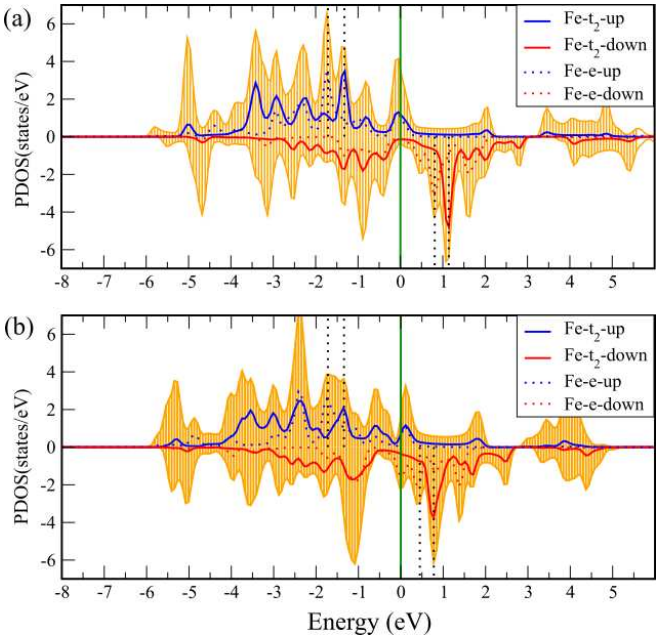

Figure 5. PDOS for Fe, e and t_2, states of (a) FeTe bulk and (b) FeTe monolayer structures. The zero of energy is set to Fermi-level.

Te we find that orbital roles in achieved the Stoner criterion. The band formed by S $3p$ orbitals is gapped at the Fermi energy, while the band formed by Se ($4p$) and Te ($5p$) orbitals is partially filled. The itinerant Se ($4p$) electrons are not big enough to satisfy the Stoner criterion, while itinerant $5p$ electrons at the Fermi energy succeeded in mediating the exchange interactions in FeTe monolayer and FeTe bulk state. It may explain why the total magnetization of the unit cell is large for FeTe bulk compares to FeTe monolayer, but zero for FeSe and FeS (See Fig. 1(c) and Fig. 4)

We have calculated this effect in our monolayer structures, FeS and FeSe, in which there is no spin-orbit coupling (SOC) effect but for FeTe, there is small SOC but not near the Fermi energy and do not affect stoner criterion which plays important role in magnetic properties of FeTe monolayer (see Fig. 4(d)).

Fig. 5 shows the PDOS of Fe, e and t_2, states of FeTe bulk and FeTe monolayer structures that result in states constituted by Fe $3d$ orbitals are very localized. The e and t_2 states are stronger hybridization for FeTe bulk as compared to the corresponding hybridization for mono-

layer. There is strong hybridization between spin up and spin down e and t_2 states at the Fermi energy in bulk case (see Fig. 5(a)), but for monolayer, there is moderate hybridization just for the e and t_2 spin-up states (see Fig. 5(b)). The amount of exchange splitting can be defined by measuring the peak shifts of the e and t_2 states for the two spin components as depicted by the vertical dotted line at Fig. 5. The asymmetric between the metallic states at the Fermi energy refers to the FeTe bulk and monolayer can be good candidates for spin filter applications.[56]

VI. CONCLUSION

In summary, we introduced FeX (X=S, Se, and Te) monolayers as structures. The stability verifications of FeS, FeSe, and FeTe monolayers in dynamical (phonon spectra), mechanical (elastic constant criteria), and thermodynamical (cohesive energy) have been studied using first principle calculations. The mechanical properties show all FeX monolayers have brittle nature. The cohesive energy per atom, charge transfer, and the work function of FeX decrease as we move down the 6A group in the periodic table, i.e., from S, Se and Te. While the bond length and bond angle and the thickness increase as we go down the 6A group. We find the magnetic moments are 3.80 μ_B and 4.67 μ_B for FeTe monolayer and bulk structures, respectively. The FeSe monolayer is nonmagnetic while the corresponding bulk is magnetic. The total magnetization of the unit cell provides the Stoner criterion which can be used to explain the difference in the magnetic moment of FeTe monolayer and bulk structures. The electronic structure of FeTe monolayer showed that it can be a beneficial structure for spin filter applications.

ACKNOWLEDGMENTS

This work was supported by the National Research Foundation of Korea (NRF) grant funded by the Korea government (MSIT) (NRF-2015M2B2A4033123).

DATA AVAILABILITY

The data that support the findings of this study are available from the corresponding author upon request.

* bafekry.asad@gmail.com; Corresponding author; bafekry.asad@gmail.com

[1] S. Chen, H. Liu, F. Chen, K. Zhou, Y. Xue, ACS Nano. 14 (2020) 11473-11481.
[2] M. Gibertini, M. Koperski, A.F. Morpurgo, K.S. Novoselov, Nat. Nanotechnol. 14 (2019) 408-419.
[3] N. D. Mermin and H. Wagner, Phys. Rev. Lett.**17**, 1133(1966).
[4] Botana, A. S. and Norman, M. R., Phys. Rev. Materials **3**, 044001 (2019).
[5] H. Li, S. Ruan, Y. Zeng, Adv. Mater. 31 (2019) 1900065.
[6] Q.H.A. Wang, K. Kalantar-Zadeh, A. Kis, J.N. Coleman, M.S. Strano, Nat. Nanotechnol. 7 (2012) 699-712.
[7] S. Manzeli, D. Ovchinnikov, D. Pasquier, O. V. Yazyev, A. Kis, Nat. Rev. Mater. 2 (2017) 17033.
[8] K. Deguchi, Y. Takano, Y. Mizuguchi, Sci. Technol. Adv. Mater. 13 (2012) 54303-54314.
[9] L. Kang, C. Ye, X. Zhao, X. Zhou, J. Hu, Q. Li, D. Liu, C.M. Das, J. Yang, D. Hu, et al.,Nat. Commun. 11 (2020) 3729.
[10] C. Gong, X. Zhang, Sci. 80, 363 (2019).
[11] B. Huang, G. Clark, E. Navarro-Moratalla, D.R. Klein, R. Cheng, K.L. Seyler, Di. Zhong, E. Schmidgall, M.A. McGuire, D.H. Cobden, et al., Nature. 546 (2017) 270-273.
[12] J.F. Ge, Z.L. Liu, C. Liu, C.L. Gao, D. Qian, Q.K. Xue, Y. Liu, J.F. Jia, Nat. Mater. 14 (2015) 285-289.
[13] Y. Deng, Y. Yu, Y. Song, J. Zhang, N.Z. Wang, Z. Sun, Y. Yi, Y.Z. Wu, S. Wu, J. Zhu, J. Wang, X.H. Chen, Y. Zhang, Nat. 563 (2018) 94-99.
[14] C. Gong, L. Li, Z. Li, H. Ji, A. Stern, Y. Xia, T. Cao, W. Bao, C. Wang, Y. Wang, Z.Q. Qiu, R.J. Cava, S.G. Louie, J. Xia, X. Zhang, Nature. 546 (2017) 265-269.
[15] F. Ma, W. Ji, J. Hu, Z.Y. Lu, T. Xiang, Phys. Rev. Lett. 102 (2009) 177003.
[16] A. Liu, X. Chen, Z. Zhang, Y. Jiang, C. Shi, Solid State Commun. 138 (2006) 538-541.
[17] Z. Wang, P. Zhang, G. Xu, L.K. Zeng, H. Miao, X. Xu, T. Qian, H. Weng, P. Richard, A. V. Fedorov, H. Ding, X. Dai, Z. Fang, Phys. Rev. B 92 (2015) 115119.
[18] A. V. Powell, P. Vaqueiro, K.S. Knight, L.C. Chapon, R.D. Sanchez, Phys. Rev. B 70 (2004) 014415.
[19] C. Koz, S. RoBler, A.A. Tsirlin, S. Wirth, U. Schwarz, Phys. Rev. B 88 (2013) 094509.
[20] X. Chen, P. Dai, D. Feng, T. Xiang, F.C. Zhang, Natl. Sci. Rev. 1 (2014) 371-395.
[21] D.S. Parker, Sci. Rep. 7 (2017) 1-6.
[22] A. Subedi, L. Zhang, D.J. Singh, M.H. Du, Phys. Rev. B 78 (2008) 134514.
[23] F. Liao, J. Swiatowska, V. Maurice, A. Seyeux, L.H. Klein, S. Zanna, P. Marcus, Appl. Surf. Sci. 283 (2013) 888-899.
[24] S. Guenon, J.G. Ramrez, A.C. Basaran, J. Wampler, M. Thiemens, I.K. Schuller, J. Supercond. Nov. Magn. 30 (2017) 297-304.
[25] X. Rui, H. Tan, Q. Yan, Nanoscale. 6 (2014) 9889-9924.
[26] M. Gong, A. Kirkeminde, N. Kumar, H. Zhao, S. Ren, Chem. Commun. 49 (2013) 9260-9262.
[27] X.J. Wu, Z.Z. Zhang, J.Y. Zhang, B.H. Li, Z.G. Ju, Y.M. Lu, B.S. Li, D.Z. Shen, J. Appl. Phys. 103 (2008) 113501.
[28] X.J. Wu, Z.Z. Zhang, J.Y. Zhang, Z.G. Ju, B.H. Li, B.S. Li, C.X. Shan, D.X. Zhao, B. Yao, D.Z. Shen, Thin Solid Films. 516 (2008) 6116-6119.
[29] R. Peng, X.P. Shen, X. Xie, H.C. Xu, S.Y. Tan, M. Xia, T. Zhang, H.Y. Cao, X.G. Gong, J.P. Hu, B.P. Xie, D.L. Feng, Phys. Rev. Lett. 112 (2014) 107001.

[30] F.C. Hsu, J.Y. Luo, K.W. Yeh, T.K. Chen, T.W. Huang, P.M. Wu, Y.C. Lee, Y.L. Huang, Y.Y. Chu, D.C. Yan, M.K. Wu, Proc. Natl. Acad. Sci. U. S. A. 105 (2008) 14262-14264.

[31] D. Liu, W. Zhang, D. Mou, J. He, Y.B. Ou, Q.Y. Wang, Z. Li, L. Wang, L. Zhao, S. He, et al., Nat. Commun. 3 (2012) 1-6.

[32] I.A. Nekrasov, N.S. Pavlov, M. V. Sadovskii, A.A. Slobodchikov, Low Temp. Phys. 42 (2016) 891-899.
L. Liu, S. Chen, Z. Lin, X. Zhang,

[33] P.K. Maheshwari, R. Jha, B. Gahtori, V.P.S. Awana, J. Supercond. Nov. Magn. 28 (2015) 2893-2897.

[34] G.F. Chen, Z.G. Chen, J. Dong, W.Z. Hu, G. Li, X.D. Zhang, P. Zheng, J.L. Luo, N.L. Wang, Phys. Rev. B 79 (2009) 140509.

[35] Y. Han, W.Y. Li, L.X. Cao, X.Y. Wang, B. Xu, B.R. Zhao, Y.Q. Guo, J.L. Yang, Phys. Rev. Lett. 104 (2010) 017003.

[36] K.D. Oyler, X. Ke, I.T. Sines, P. Schiffer, R.E. Schaak, Chem. Mater. 21 (2009) 3655-3661.

[37] P.D. Matthews, M. Akhtar, M.A. Malik, N. Revaprasadu, P. O Brien, Dalt. Trans. 45 (2016) 18803-18812.

[38] K. Shigekawa, K. Nakayama, M. Kuno, G.N. Phan, K. Owada, K. Sugawara, T. Takahashi, T. Sato, Proc. Natl. Acad. Sci. 116 (2019) 24470 LP - 24474.

[39] S. He, J. He, W. Zhang, L. Zhao, D. Liu, X. Liu, D. Mou, Y.B. Ou, Q.Y. Wang, Z. Li, et al.,Nat. Mater. 12 (2013) 605-610.

[40] X. Lai, H. Zhang, Y. Wang, X. Wang, X. Zhang, J. Lin, F. Huang, J. Am. Chem. Soc. 137 (2015) 10148-10151.

[41] J. Paglione, R.L. Greene, Nat. Phys. 6 (2010) 645-658.

[42] J. P. Perdew, K. Burke, and M. Ernzerhof, Phys. Rev. Lett. **77**, 3865 (1996).

[43] J. P. Perdew, K. Burke, and M. Ernzerhof, Phys. Rev. Lett. **78**, 1396 (1997).

[44] G. Kresse and J. Hafner, Phys. Rev. B **47**, 558 (1993).

[45] G. Kresse and J. Hafner, Phys. Rev. B **49**, 14251 (1994).

[46] H.J. Monkhorst and J.D. Pack, Phys. Rev. B **13**, 12, (1976).

[47] G. Henkelman, A. Arnaldsson, and H. Jonsson, Comput. Mater. Sci. **36**, 354 (2006).

[48] S. J. Grimme, Comput. Chem. **27**, 1787 (2006).

[49] D. Alfe, Comput. Phys. Commun. **180**, 2622 (2009).

[50] Kang, Lixing and Ye, Chen and Zhao, Xiaoxu and Zhou, Xieyu and Hu, Junxiong and Li, Qiao and Liu, Dan and Das, Chandreyee and Yang, Jiefu and Hu, Dianyi, et al.,Nat. Comm. **11**, 3729 (2020).

[51] Subedi, Alaska and Zhang, Lijun and Singh, D. J. and Du, M. H., Phys. Rev. B **78**, 134514 (2008).

[52] H. Rojas-Chavez, H. Cruz-Martinez, E. Flores-Rojas, J.M. Juarez-Garcia, J.L. Gonzalez-Dominguez, N. Daneu, J. Santoyo-Salazar, Phys. Chem. Chem. Phys. **20**, 27082 (2018).

[53] R. Hill, The Elastic Behaviour of a Crystalline Aggregate, Proc. Phys. Soc., London, Sect. A **65**, 349 (1952).

[54] S. F. Pugh, XCII. Philos. Mag. **45**, 823 (1954).

[55] W. C. Hu , Y. Liu , D. J. Li , X. Q. Zeng and C. S. Xu, Comput. Mater. Sci. **83**, 27 (2014).

[56] M. M Fadlallah and A. A. Maarouf and U. Schwingenschlogl and U. Eckern, J. Phys.: Condens. Matter **29**, 055301 (2016).